symmetry

MDPI

Article

The Symmetric 3D Organization of Connective Tissue around Implant Abutment: A Key-Issue to Prevent Bone Resorption

Giovanna Iezzi [1], Francesca Di Lillo [2], Michele Furlani [3], Marco Degidi [4], Adriano Piattelli [1,5,6,7] and Alessandra Giuliani [3,*]

1 Department of Medical, Oral and Biotechnological Sciences, University of Chieti-Pescara, 66100 Chieti, Italy; gio.iezzi@unich.it (G.I.); apiattelli@unich.it (A.P.)
2 Elettra Sincrotrone Trieste S.C.P.A, 34149 Basovizza, Italy; francesca.dilillo@elettra.eu
3 Department of Clinical Sciences, Polytechnic University of Marche, 60131 Ancona, Italy; m.furlani@pm.univpm.it
4 Private Practice, 40139 Bologna, Italy; info@degidi.it
5 Fondazione Villaserena per la ricerca, 65013 Città Sant'Angelo, Italy
6 Casa di Cura Villa Serena, 65013 Città Sant'Angelo, Italy
7 Chair of Biomaterials Engineering, Catholic University of San Antonio of Murcia (UCAM), 30107 Guadalupe, Spain
* Correspondence: a.giuliani@univpm.it; Tel.: +39-0712204603

Abstract: Symmetric and well-organized connective tissues around the longitudinal implant axis were hypothesized to decrease early bone resorption by reducing inflammatory cell infiltration. Previous studies that referred to the connective tissue around implant and abutments were based on two-dimensional investigations; however, only advanced three-dimensional characterizations could evidence the organization of connective tissue microarchitecture in the attempt of finding new strategies to reduce inflammatory cell infiltration. We retrieved three implants with a cone morse implant–abutment connection from patients; they were investigated by high-resolution X-ray phase-contrast microtomography, cross-linking the obtained information with histologic results. We observed transverse and longitudinal orientated collagen bundles intertwining with each other. In the longitudinal planes, it was observed that the closer the fiber bundles were to the implant, the more symmetric and regular their course was. The transverse bundles of collagen fibers were observed as semicircular, intersecting in the lamina propria of the mucosa and ending in the oral epithelium. No collagen fibers were found radial to the implant surface. This intertwining three-dimensional pattern seems to favor the stabilization of the soft tissues around the implants, preventing inflammatory cell apical migration and, consequently, preventing bone resorption and implant failure. This fact, according to the authors' best knowledge, has never been reported in the literature and might be due to the physical forces acting on fibroblasts and on the collagen produced by the fibroblasts themselves, in areas close to the implant and to the symmetric geometry of the implant itself.

Keywords: bone resorption; X-ray microtomography; histological techniques; dental implants; connective tissue; fibroblasts; inflammatory cells; symmetric 3D organization

Citation: Iezzi, G.; Di Lillo, F.; Furlani, M.; Degidi, M.; Piattelli, A.; Giuliani, A. The Symmetric 3D Organization of Connective Tissue around Implant Abutment: A Key-Issue to Prevent Bone Resorption. *Symmetry* **2021**, *13*, 1126. https://doi.org/10.3390/sym13071126

Academic Editors: Monika Martiniaková, Birgit Grosskopf and Chiarella Sforza

Received: 26 April 2021
Accepted: 11 June 2021
Published: 24 June 2021

1. Introduction

Soft tissues, which surround the transmucosal part of dental implants, ensure healthy conditions, stable osseointegration and long-term implant success and survival. They are called "peri-implant mucosa" [1] and were proved to be a biological seal preventing the development of inflammatory peri-implant diseases. Indeed, well-organized connective tissues around the implant were hypothesized to decrease early bone resorption by reducing inflammatory cell infiltration.

Morphology and structure of the connective tissue barrier around the implants have been investigated in animals [2,3] and in humans [4–9].

It is well-known that the implant–connective-tissue interface is different from periodontal connective tissue [10], with different arrangements of collagen fibers around the implant. Circular fibers have more frequently been observed [11–14], but also fibers parallel to the longitudinal axis of the implant, i.e., running in the apico-coronal direction [14,15] and, in a few cases, fibers inserting onto the implant surface [16].

Connective tissues are challenging to detect by X-ray tomography because of their low dimension and density; indeed, the previous studies that referred to the connective tissue around implant abutments were based on two-dimensional (2D) investigations, mainly histological evaluations [8,17]. However, only advanced three-dimensional (3D) characterizations could enhance the knowledge of connective tissue architecture in the attempt of finding new strategies to reduce inflammatory cell infiltration with the consequent decrease of early bone resorption.

In this framework, X-ray phase-contrast imaging may represent a powerful method to study the 3D organization of connective tissue around the abutments, as it allowed to achieve reliable 3D imaging, with increased contrast, of several organs/tissues [18].

In this context, in the last ten years, we started to study the extracellular matrix (ECM) by synchrotron radiation-based high-resolution phase-contrast tomography (SR-PhC-microCT). SR-PhC-microCT was successful in detecting, with high spatial resolution, the 3D structural organization of ECM within bioscaffolds, supporting the understanding of how the presence of cells modified the construct arrangement [19,20]. Moreover, we recently performed SR-PhC-microCT on uterine leiomyomas, demonstrating the capability of this method to discriminate healthy and pathologic collagen distribution in this district without using contrast agents [21].

Thus, we tested in the present demonstrative study, for the first time to the authors' knowledge, the combined use of phase-contrast imaging and light microscopy to reliably reconstruct the 3D organization of connective tissue around the neck of dental implants. A secondary aim was to evaluate how physical forces drive collagen organization, supporting the stabilization of soft tissues and, consequently, decreasing the possibility of bone resorption and implant failure.

2. Materials and Methods

2.1. Sample description and Ethical Committee Approval

The archives of the Dental School of the University of Chieti-Pescara, Italy, were searched for human retrieved implants with the presence of peri-implant soft tissues. Three implants with a cone morse implant–abutment connection (Ankylos, Dentsply-Friadent, Mannheim, Germany) were considered. These specimens had already been studied [6–8]; they had been inserted in an equicrestal location, immediately loaded, and retrieved after 4–6 weeks. The implants have been removed for psychological distress and because they were part of a human protocol, approved by the Ethical Committee of the University of Guarulhos, Sao Paulo, Brasil.

The implants were well osseointegrated and stable before retrieval. No inflammation of the peri-implant soft tissues was present.

The use of these specimens for these scientific purposes has been approved by the Ethical Committee of the University of Chieti-Pescara (CODE: BONEISTO, 15 September 2019).

The samples have been previously fixed by immersion in 10% buffered formalin, dehydrated in an increasing series of alcoholic rinses, embedded in glicol-methacrylate resin (Technovit 7200 VLC; Kulzer, Wehrheim, Germany) and stored in the archives. After retrieving from the archives, they were processed to be analyzed by histology and SR-PhC-microCT. In particular, the specimens were sectioned along their longitudinal axis in order to obtain some small portions. A portion was examined by SR-PhC-microCT after removal of the abutment, and subsequently, it was sectioned along its longitudinal axis for the histological evaluation. Another portion of the implant was used to obtain the sections transversal or perpendicular to the major axis of the abutment.

2.2. Histology

For the histological evaluation, longitudinal and transversal sections were obtained.

Histological analysis was carried out under a light microscope (Laborlux S, Leitz, Wetzlar, Germany) connected to a high-resolution video camera (3CCD, JVCKY-F55B, JVC, Yokohama, Japan) and interfaced with a PC. This optical system was associated with a digitizing pad (Matrix Vision GmbH, Oppenweiler, Germany) and a histomorphometry software package with image capturing capabilities (Image-Pro Plus 4.5, Media Cybernetics Inc., Immagini and Computer Snc, Milano, Italy). One single well-trained examiner (GI), not involved in the surgical treatment, evaluated the histological results.

2.3. Polarized Light

Birefringence, obtained by polarized light microscopy, was evaluated to obtain information on the orientation of the collagen bundles. Thin transversal sections of the tissue were observed using an Axiolab optical microscope (Laborlux S, Leitz, Wetzlar, Germany). This instrument was equipped with two linear polarizers and two quarter-wave plates arranged to transmit circularly polarized light. The collagen bundles that were transversely aligned to the light propagation direction, i.e., that were parallel to the section plane, appeared bright because of the variation of the existing light refraction, while the collagen fibers aligned along the light propagation axis, i.e., perpendicular to the plane of the section, appeared in a different color because refraction did not occur.

2.4. Synchrotron Radiation-Based Phase-Contrast Microtomography

The microCT scanning was performed at the SYRMEP beamline of the ELETTRA Synchrotron Facility (Basovizza, TS, Italy). Synchrotron radiation (SR) microCT is usually based on conventional settings, i.e., on attenuation properties of tissues inside the sample, that are related to the β value, i.e., to the complex part of the index of refraction $n = 1 - \delta + i\beta$. However, because of the coherence of synchrotron light, we can also exploit the phase shift term δ that is related to the electron density of the tissues inside the sample [22]. This latter approach is preferable when different tissues in a biopsy have similar electron densities or negligible X-ray absorption: in these cases, with the reconstruction of δ distribution, image contrast, image segmentation and the subsequent quantitative analysis are significantly improved. In the present study, we used this last method to study the 3D organization of the collagen around the neck of dental implants.

The scans were performed using the pink beam delivered by the synchrotron facility, filtered by a 0.5-mm thick silicon plate, producing an X-ray beam with an average energy of 19 keV. We used 0.2 s of exposure time per projection over a total range of 180°; the sample–detector distance was set to 100 mm, resulting in an 890 nm isotropic pixel size of the projections. The tomographic reconstruction was performed with the SYRMEP Tomo Project (STP) open-source software [23], using Paganin's method for the phase retrieval algorithm, aiming to reconstruct the decrement δ of the refractive index n [24]. Paganin's method realizes the phase retrieval by assuming a linear relationship between the absorption index β and the refractive index decrement δ that is acceptable if samples are homogenous and propagation distances are in the near field regime. The adopted scans geometries and the investigated connective tissues fulfill the previous conditions. The δ/β ratio was set to 100.

Afterward, the commercial software VG Studio MAX 1.2 (Volume Graphics, Heidelberg, Germany) and the open-source ImageJ software (imagej.nih.gov/ij, accessed on 26 April 2021) were used to generate 3D images and sequences of longitudinal and transversal 2D slices, where grey levels were proportional physical density distribution of the tissue.

The morphometric evaluation of collagen bundles was performed by exploiting the structural indices usually measured in bone samples [25]: collagen specific volume (CollV/TV, expressed as a percentage), mean collagen bundle thickness (CollTh, expressed in micrometers), mean collagen bundle number (CollNr, per millimeter) and mean collagen

bundle spacing (CollSp, expressed in micrometers). Furthermore, as collagen bundles could vary their orientation in the transversal or longitudinal direction and at different distances from the implant, information about the presence of preferential orientation(s) was also extracted. Indeed, the anisotropy degree index (DA) measures how much a structure is oriented and varies between 0, representing all observations confined to a single plane or axis, and 1, corresponding to the perfect isotropy. We also calculated the interconnectivity of the collagen bundles, measuring the connectivity density parameter (Conn.D, expressed as pixel^{-3}), which is a global measure giving higher values for better-connected bundles and lower values for poorly connected ones. Furthermore, we studied the collagen bundles' shape and 3D complexity; indeed, using the fractal theory, it is possible to quantify structures with complex form through the fractal dimension, which is a parameter indicating to what extent an irregular structure tends to fill space, with analysis at different scales. The box-counting dimension has been used because of its easy implementation [26] with the following settings: starting box size (px): 48, smallest box size (px): 6; box scaling factor: 1.2; grid translations: 0. The complete morphometric analysis, including DA, Conn.D, and 3D Fractal Dimension data, was performed using the BoneJ Plugin of the ImageJ software, version 3 (https://imagej.net/plugins/bonej, accessed on 26 April 2021).

3. Results

Before analysis, abutments were removed in order to enable synchrotron investigation.

3.1. Histology

The histological analysis of the peri-implant soft tissues showed that the biological width (BW) was composed of sulcular epithelium (SE), which continued with junctional epithelium (JE) and was in close contact with the implant surface. JE was composed of a layer of epithelial cells that had adhered to the surface of the transmucosal collar. The most apical part of JE ended by decreasing in thickness. Below the JE, the connective tissue (CT) detached from the surface during the implant retrieval, showing dense fibrous tissue with some blood vessels (Figure 1).

3.2. Polarized Light

Polarized light microscopy showed that the peri-implant mucosa was constituted by different collagen bundles, distinguishable both in longitudinal and transversal sections. Analyzing the soft tissues, from the implant surface towards the portion most distant from it, it was observed that the bundle distribution was more recognizable in the portion near the surface, while they were less identifiable in the most distant portion.

The transversal sections performed in the CTP area, as indicated in Figure 1: the blue color indicated the collagen fibers parallel to the long axis of the implant–abutment unit, whereas the yellow color showed the collagen fibers that run perpendicularly or circularly to the implant–abutment unit (Figure 2a).

Longitudinal sections representative of the CT area (Figure 2d): the yellow color represents the parallel collagen fibers in relation to the long axis of the implant–abutment; whereas the blue color showed the collagen fibers that run perpendicular in relation to the section plane (circularly around the implant–abutment unit).

Analyzing a large portion of the cross-sections performed in the CTP area, as indicated in Figure 1 (areas $\geq 1/4$ of the abutment circumference), of the peri-implant soft tissue, several details on the orientation of the transverse fibers were detected.

In the connective tissue portion, collagen fibers running perpendicular to the longitudinal axis of the implant–abutment unit showed a semicircular orientation. In fact, they ran around the abutment following its circular profile and then finished by anchoring themselves to the oral epithelium (Figure 3a,c).

By reconstructing the semicircular orientation of the collagen fibers around the transversal abutment profile, it was possible to observe how the semicircular fibers coming

from different collagen bundles intersected with each other, as described in the concept drawings (Figure 3b,d).

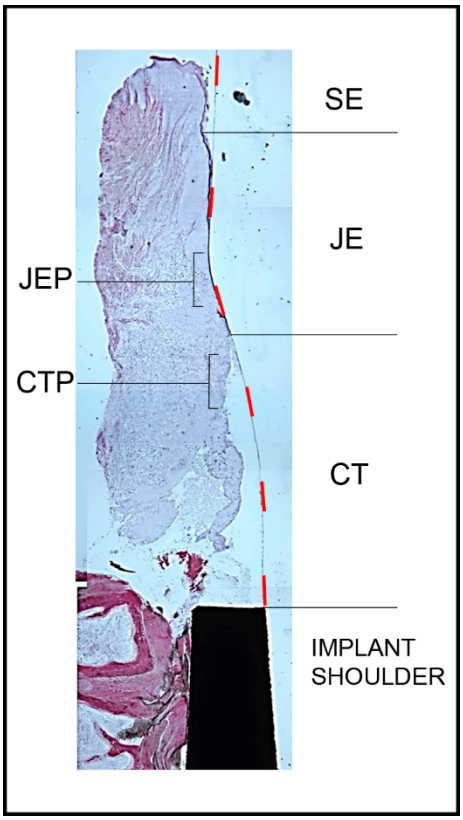

Figure 1. Histological section of the implant–abutment unit. Peri-implant soft tissues were composed of sulcular epithelium (SE), junctional epithelium (JE)—which was in close contact with the implant surface—and connective tissue (CT) detached from the surface during the implant retrieval. The junctional epithelium portion (JEP) and the connective tissue portion (CTP) indicated the position in which the transversal sections were obtained (Acid fuchsin-Toluidine blue 20X).

3.3. Synchrotron Radiation-Based Phase-Contrast Microtomography

Representative 2D slices and details of the test sample are shown in Figure 2: transversal (Figures 2b and 4) and longitudinal planes (Figure 2e) were considered in order to reconstruct the exact collagen bundles distribution in the 3D space. Stack-sequences of 2D transversal (250 frames of around 3.2×10^6 μm^2) and longitudinal (2000 frames of around 0.4×10^6 μm^2) slices have been respectively reported in Video S1 and S2 in the Supplementary Materials section.

The biopsy revealed a regular pattern of the collagen bundles: they were shown, by PhC-microCT 3D observations, to be made of circular (C-CB) and longitudinal (L-CB) fibers. No radial collagen fibers with respect to the implant surface were observed. Circular fibers were confirmed to be the most numerous [9] and, differently with respect to other observations [5], they were not located externally. The longitudinal fibers were located internally, but an intertwining between the bundles of circular and longitudinal fibers was observed, as described in the concept drawings (Figure 2c,f), and in Figure 4. Moreover, few blood vessels were found, as shown in Figures 2 and 4, both in the transversal (Figures 2b,c and 4) and longitudinal planes (Figure 2e,f).

The 3D microarchitecture of the collagen bundles was also investigated by a quantitative morphometric approach. After a process of contrast enhancing, a median (radius = 4 pixels) filter was used in order to homogenize the collagen bundles signal, decreasing the noise at the same time. Afterward, a threshold of 161 (8 bit scale: 0–255) was selected in order to eliminate all the other phase signals (endothelium, cells, etc.)

with the exception of the collagen-phase. Therefore, several subvolumes in the test biopsy were analyzed, each of around 19×10^6 μm^3: the complete set of them allowed to map the full biopsy. Data analysis was reported in Table 1. Collagen bundles in transversal planes (Transversal_CB), due to the reduced thickness of the biopsies in this direction, were considered as a single shell of collagen bundles. Instead, the mean thickness of biopsies in the longitudinal direction was higher (around 500 μm), allowing the discrimination of two shells, the inner (Longitudinal_CB-inner) and the outer (Longitudinal_CB-outer), each with a mean thickness equal to 250 μm.

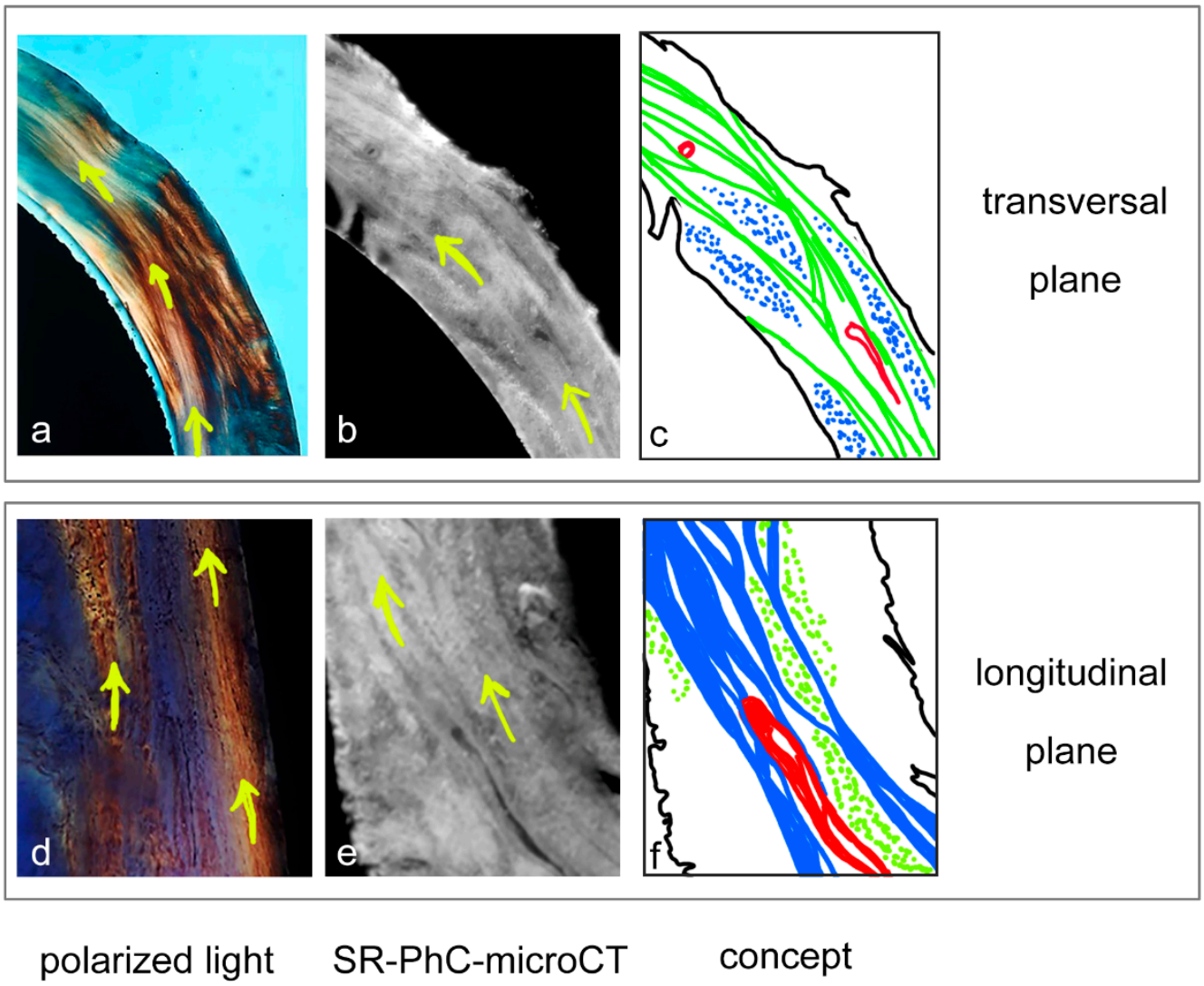

Figure 2. Polarized light and synchrotron-based microtomography in the connective tissue portion (CTP): from the combined imaging to the concept. (**a**,**d**) Polarized light evidence: (**a**) transversal section of the peri-implant soft tissue in the coronal portion of the implant: the pale yellow color indicated the collagen fibers that run circularly around the implant (yellow arrows), whereas the blue color showed the collagen fibers parallel to the long axis of the implant; (**d**) longitudinal section of the peri-implant soft tissue in the coronal portion of the implant: the junctional epithelium was in close contact with the implant surface. No inflammatory infiltrate was observed. Yellow color represented the collagen fibers parallel to the long axis of the implant–abutment (yellow arrows), whereas the blue color showed the collagen fibers that run to the long axis of the implant (circularly around the implant–abutment unit); (**b**,**c**–**e**,**f**) synchrotron radiation-based phase-contrast microtomography: (**b**) sampling 2D slice in a transversal plane; (**c**) concept drawing describing structures in the panel-b slice: circular collagen bundles (green lines), with evidence of interlaced longitudinal collagen bundles (blue spots) and few vessels (red structures); (**e**) sampling of a 2D slice in a longitudinal plane; (**f**) concept drawing describing structures in panel-e slice: longitudinal collagen bundles (blue lines) with evidence of interlaced circular collagen bundles (green spots) and few vessels (red structures).

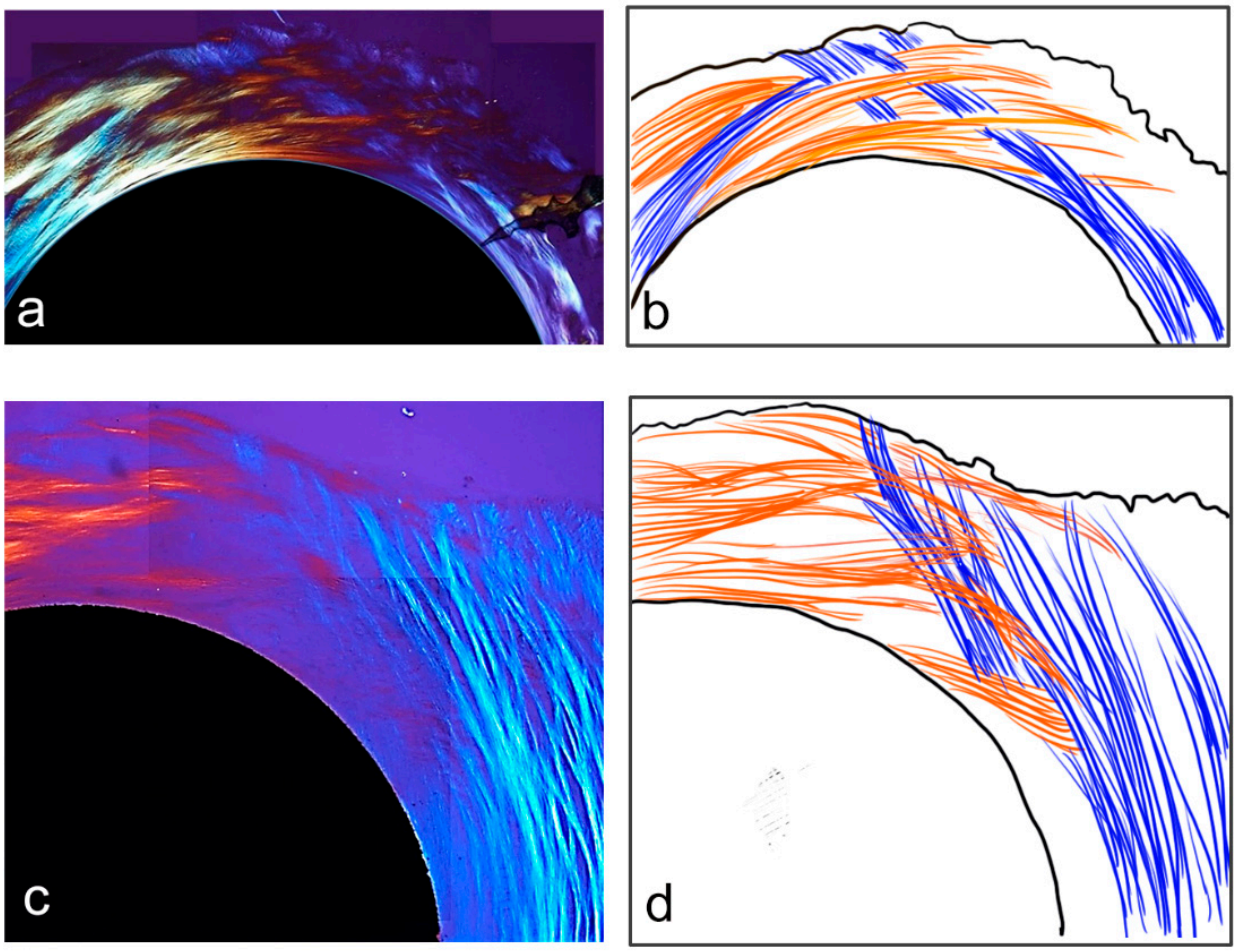

Figure 3. Evidence of semicircular orientation for transversal collagen bundles in the connective tissue portion (CTP). (**a**–**c**) Polarized light evidence: transversal section reconstructions of the peri-implant soft tissue surrounding at least an area $\geq 1/4$ of the abutment circumference. The transverse collagen bundles ran perpendicularly to the long axis of the implant–abutment unit and showed a semicircular orientation. Indeed, they ran around the abutment partially following its circular profile and then finished by anchoring to the soft tissues; (**b**–**d**) conceptual drawings describing how different collagen bundles (blue lines and red lines) intersect with each other.

Table 1. Collagen bundles three-dimensional morphometric analysis in the retrieved biopsies. Mean values ± standard deviation. Transversal CB: morphometric analysis of circular (transversal) collagen bundles; Longitudinal CB—inner: morphometric analysis of the inner shells of the transversal collagen bundles; Longitudinal CB—outer: morphometric analysis of the outer shells of the transversal collagen bundles. Mean thickness (mTh) of the biopsy in the transversal plane: 300 µm; mTh of the inner shells in the longitudinal plane: 250 µm; mTh of the outer shells in the longitudinal plane: 250 µm.

	Transversal CB mTh: 300 µm	**Longitudinal CB—Inner mTh: 250 µm**	**Longitudinal CB—Outer mTh: 250 µm**
CollV/TV (%)	35 ± 25	38 ± 6	51 ± 10
CollTh (µm)	33 ± 15	36 ± 6	47 ± 11
CollNr (mm^{-1})	9 ± 2	10 ± 1	10 ± 2
CollSp (µm)	78 ± 38	64 ± 10	52 ± 16
DA	0.70 ± 0.20	0.61 ± 0.04	0.67 ± 0.05
Conn.D ($\times 10^{-6}$) (px^{-3})	10.4 ± 5.3	13.4 ± 3.3	13.3 ± 4.4
3D Fractal Dimension	2.35 ± 0.07	2.39 ± 0.02	2.42 ± 0.07

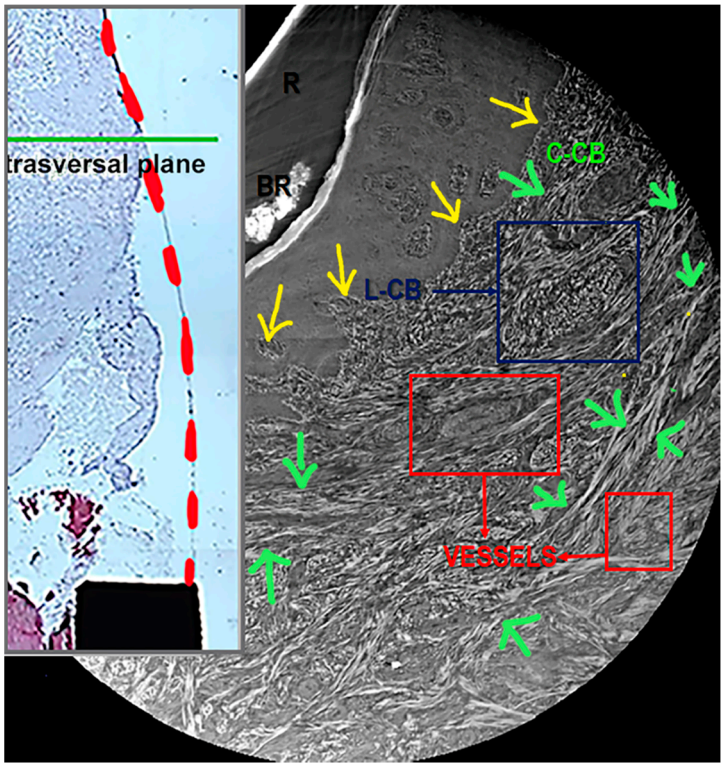

Figure 4. Synchrotron radiation-based phase-contrast microtomography in the junctional epithelium portion (JEP): transversal 2D slice in a sampling plane, as indicated (green line) in the top-left insert (focus of the histological longitudinal slice in Figure 1). Red dashed line: abutment interface before removal. Circular collagen bundles (C-CB) are indicated by the green arrows, with evidence of interlaced longitudinal collagen bundles (L-CB) and few vessels (V). Yellow arrows show the interface between connective tissue (CT) and junctional epithelium (JE). RB: residuals of bone; R: resin.

No relevant morphometric differences between the three groups (Transversal, Longitudinal_CB-inner and Longitudinal_CB–outer) were found; indeed, the data in Table 1 showed that the distributions of collagen bundles were similar, in terms of volume (CollV/TV), average thickness (CollTh), number (CollNr) and distance (CollSp), comparing Transversal_CB and Longitudinal_CB–inner. However, higher mismatches have been detected between Longitudinal_CB–inner and Longitudinal_CB-outer observations. Indeed, the Longitudinal_CB–outer was found to have thicker and closer bundles than Longitudinal_CB–inner, as also shown in the concept drawing in Figure 2f.

Interestingly, three other results were obtained, as detailed in Table 1:

- Although the number of samples analyzed was comparable, the standard deviation of data obtained for Transversal_CB was always higher than for Longitudinal_CB and the standard deviation of data obtained for Longitudinal_CB-outer was always higher than for Longitudinal_CB-inner;
- The anisotropy degree (DA) in Transversal_CB was always lower (higher DA values) than for Longitudinal_CB;
- The connectivity density (Conn. D) and the 3D fractal dimension were lower in Transversal_CB than in Longitudinal_CB.

In general, these three results revealed large structural inhomogeneity in Transversal_CBs and slight differences between the inner and the outer shells of the Longitudinal_CBs.

4. Discussion

It has been observed that the subcrestal connective tissue in animal studies was characterized by a three-dimensional network of collagen bundles, running in different directions [27]; however, to date, the network of collagen bundles has always been analyzed

with two-dimensional techniques, hampering a full comprehension of their 3D organization. Therefore, in this study, different techniques, including 3D methods, were combined in order to analyze the organization of collagen around the collar.

Indeed, under polarized light microscopy, the collagen fiber orientation mainly showed two directions, parallel and perpendicular to the long axis of the implant [8,17]. More specifically, the analysis of big portions of the soft tissues surrounding the abutment circumference in transversal sections showed a semicircular trend of the fibers. In fact, the different transverse bundles of collagen fibers followed its circular profile and then finished by anchoring themselves to the oral epithelium. These results were similar to the study conducted by Rodríguez [9], where, however, circular fibers were observed in the apical portion of the abutment, while, in the present study, the transverse bundles of collagen fibers were semicircular, and they intersected each other in the lamina propria of the mucosa and ended in the oral epithelium. This organization, not reported in literature to date, could favor the stability of the connective tissue.

So far, tissue tension during wound healing processes was attributed to forces produced by fibroblasts alone; however, in situ monitoring of tissue forces together with second harmonic imaging recently indicated a mechanical contribution of tensioned collagen fibrils in the contraction process [28]. Therefore, our analysis has also been focused on the mechanical action of collagen around the transmucosal implant collar.

In the present study, the propagation-based phase-contrast microCT was used, for the first time to the authors' knowledge, to evaluate the collagen amount and 3D distribution in peri-implant mucosa: collagen fibers with circular and longitudinal orientation, but no radial orientation with respect to the implant, were also observed by this method; no significant differences in term of volume, thickness and number of collagen bundles in the transversal compared to longitudinal planes were found. However, in the longitudinal planes, it was observed that the closer the fiber bundles were to the implant, the more regular this pattern was (increasing DA from inner shells to outer ones).

Moreover, the interconnectivity of the collagen structure was observed to be lower in Transversal_CB than in Longitudinal_CB, justifying the increase of resistance to loading stress in the longitudinal with respect to transversal direction.

The analysis of the 3D fractal dimension of the collagen bundles is the real novelty of the present study. In recent years, a restricted number of studies have focused on the 3D complexity of the trabecular bone network by means of the extension of the box-counting algorithm to 3D reconstructions obtained from microCT and MRI images [29]. However, to date, none of them have dealt with the 3D fractal dimension of soft tissues in the dental area. It has been observed that, even if not significantly, the 3D Fractal Dimension was lower in Transversal_CB than in Longitudinal_CB and for Longitudinal_CB-inner than for Longitudinal_CB-outer, confirming a concept previously observed with the study of the interconnectivity and of the anisotropy degree, i.e., that the closer the collagen bundles were to the implant, the more regular this pattern was.

The present study should be considered prevalently as a set-up of a new methodology because it has the limit that the evaluation has been done on a very limited number of specimens; however, our investigation provides novel evidence that structural properties of collagen bundles around the neck of a dental implant could give an indication on how physical forces drive their 3D organization and stability around the implant collar. Indeed, one of the main known functions of the collagen bundles is to take over the mechanical load [30]: the bundles thickness determines whether fibers may creep (like in lung, nerves or cornea) or transfer high loads (like in tendons) [31]. Moreover, the collagen bundles were shown to be preferentially aligned in the main load-bearing directions; consequently, the dimension and orientation of the collagen bundles play an important role in tissue stability [32].

In order to understand how physical forces drive collagen bundles' 3D organization and stability, it is fundamental to understand the mechanisms by which tensile forces support wound closure in implantology. Up until ten years ago, tissue tension was at-

tributed to cellular forces produced by resident fibroblasts alone [33]. However, a recent study showed, by an in vitro wound healing model, that the storage of tensile forces in the extracellular matrix has a significant contribution to macroscopic tissue tension [28]. In particular, it was shown that the distributions of collagen fibrils correlated with tissue contraction, demonstrating a mechanical contribution of tensioned collagen bundles in the wound healing.

In the present demonstrative study, it has been shown that collagen bundles were oriented circularly and longitudinally with respect to the implant neck, within an intertwining 3D pattern. This 3D organization was most likely due, as suggested in the recent literature, to tensile forces acting during wound healing [28]. Indeed, during surgical implantation, a wound is always created; fibroblasts were shown to migrate towards the implant anchoring to the titanium surface, with forces and modalities depending on the biomaterial composition and roughness [34]. However, cells incrementally deposit tensioned collagen fibrils, which leads to a gradual increase in the total force resulting in local compression perpendicularly to the implant surface. The extracellular matrix and, in particular, the collagen fibers production were shown to follow the cell anchorage [19,20,35,36], i.e., parallel to the implant neck surface. Hence, because of the axial symmetry of the implant neck, the collagen bundles seemed to organize themselves circularly around the implant in the transversal direction and longitudinally following the axial profile of the neck, but not radially, as we observed.

However, the possible influence of the surgical procedure should be explored more in-depth, with quantitative evaluation on more specimens and even in patients suffering from peri-implantitis, at different stages of this disease.

In conclusion, this study defines a new paradigm in the implantology scenario: implant success is no longer only linked to the management of the bone–implant interface but is also highly dependent on the abundance and distribution of collagen bundles generated during the first wound healing phase.

Supplementary Materials: The following are available online at https://www.mdpi.com/article/10.3390/sym13071126/s1, Video S1: SR-PhC-microCT stack-sequence of 2D transversal (250 frames of around 3.2×10^6 μm^2) slices; Video S2: SR-PhC-microCT stack-sequence of 2D longitudinal (2000 frames of around 0.4×10^6 μm^2) slices.

Author Contributions: Conceptualization, G.I., A.P. and A.G.; methodology, G.I. and A.G.; software, M.F., F.D.L.; validation, M.D.; formal analysis, G.I. and A.G.; investigation, F.D.L., M.F.; resources, M.D. and A.P.; data curation, M.D.; writing—original draft preparation, G.I., A.P., M.F. and A.G.; writing—review and editing, M.F. and A.G.; visualization, M.F.; supervision, G.I., A.P. and A.G.; project administration, A.P.; funding acquisition, A.P. All authors have read and agreed to the published version of the manuscript.

Funding: This research received no external funding with the exception of the synchrotron experiments for which travel and subsistence at ELETTRA were funded by the Program "Support to the Italian Users of ELETTRA". No other sources of study funding were used.

Institutional Review Board Statement: The study was conducted according to the guidelines of the Declaration of Helsinki, and approved by the Ethics Committee of the University of Chieti-Pescara (CODE: BONEISTO, 15 September 2019).

Informed Consent Statement: Informed consent was obtained from all subjects involved in the study.

Data Availability Statement: Histological and morphometric data are contained within the article. The complete SR-PhC-microCT set of data presented in this study are available on request from the corresponding author; indeed, they are not publicly available due to their extremely large size.

Acknowledgments: Authors thank the ELETTRA Synchrotron Facility for the allocated beamtime at the SYRMEP beamline.

Conflicts of Interest: The authors declare no conflict of interest.

References

1. Lindhe, J.; Meyle, J.; on behalf of Group D of the European Workshop on Periodontology. Peri-implant diseases: Consensus Report of the Sixth European Workshop on Periodontology. *J. Clin. Periodontol.* **2008**, *35*, 282–285. [CrossRef] [PubMed]
2. Berglundh, T.; Lindhe, J.; Jonsson, K.; Ericsson, I. The topography of the vascular systems in the periodontal and peri-implant tissues in the dog. *J. Clin. Periodontol.* **1994**, *21*, 189–193. [CrossRef] [PubMed]
3. Moon, I.-S.; Berglundh, T.; Abrahamsson, I.; Linder, E.; Lindhe, J. The barrier between the keratinized mucosa and the dental implant. *J. Clin. Periodontol.* **1999**, *26*, 658–663. [CrossRef] [PubMed]
4. Piattelli, A.; Scarano, A.; Bertolai, R.; Panzoni, E.; Piattelli, M. Histologic Aspects of the Bone and Soft Tissues Surrounding Three Titanium Non-Submerged Plasma-Sprayed Implants Retrieved at Autopsy: A Case Report. *J. Periodontol.* **1997**, *68*, 694–700. [CrossRef]
5. Schierano, G.; Ramieri, G.; Cortese, M.; Aimetti, M.; Preti, G. Organization of the connective tissue barrier around long-term loaded implant abutments in man. *Clin. Oral Implant. Res.* **2002**, *13*, 460–464. [CrossRef]
6. Degidi, M.; Iezzi, G.; Scarano, A.; Piattelli, A. Immediately loaded titanium implant with a tissue-stabilizing/maintaining design ('beyond platform switch') retrieved from man after 4 weeks: A histological and histomorphometrical evaluation. A case report. *Clin. Oral Implant. Res.* **2008**, *19*, 276–282. [CrossRef]
7. Degidi, M.; Perrotti, V.; Shibli, J.A.; Novaes, A.B.; Piattelli, A.; Iezzi, G. Equicrestal and Subcrestal Dental Implants: A Histologic and Histomorphometric Evaluation of Nine Retrieved Human Implants. *J. Periodontol.* **2011**, *82*, 708–715. [CrossRef]
8. Degidi, M.; Piattelli, A.; Scarano, A.; Shibli, J.A.; Iezzi, G. Peri-implant collagen fibers around human cone Morse connection implants under polarized light: A report of three cases. *Int. J. Periodontics Restor. Dent.* **2012**, *32*, 323–328.
9. Rodríguez, X.; Navajas, A.; Vela, X.; Fortuño, A.; Jimenez, J.; Nevins, M. Arrangement of Peri-implant Connective Tissue Fibers Around Platform-Switching Implants with Conical Abutments and Its Relationship to the Underlying Bone: A Human Histologic Study. *Int. J. Periodontics Restor. Dent.* **2016**, *36*, 533–540.
10. Romanos, E.G.; Schröter-Kermani, C.; Weingart, D.; Strub, J.R. Health human periodontal versus peri-implant gingival tissues: An immunohistochemical differentiation of the extracellular matrix. *Int. J. Oral Maxillofac. Implant.* **1995**, *10*, 750–758.
11. Rompen, E.; Domken, O.; Degidi, M.; Pontes, A.E.F.; Piattelli, A. The effect of material characteristics, of surface topography and of implant components and connections on soft tissue integration: A literature review. *Clin. Oral Implant. Res.* **2006**, *17*, 55–67. [CrossRef]
12. Rugger, A.; Franchi, M.; Marini, N.; Trisi, P.; Piattelli, A. Supracrestal circular collagen fiber network around osseointegrated nonsubmerged titanium implants. *Clin. Oral Implant. Res.* **1992**, *3*, 169–175. [CrossRef]
13. Rodríguez, X.; Vela, X.; Calvo-Guirado, J.L.; Nart, J.; Stappert, C.F.J. Effect of platform switching on collagen fiber orientation and bone resorption around dental implants: A preliminary histologic animal study. *Int. J. Oral Maxillofac. Implant.* **2012**, *27*, 1116–1122.
14. Sculean, A.; Gruber, R.; Bosshardt, D.D. Soft tissue wound healing around teeth and dental implants. *J. Clin. Periodontol.* **2014**, *41*, S6–S22. [CrossRef]
15. Abrahamsson, I.; Berglundh, T.; Glantz, P.-O.; Lindhe, J. The mucosal attachment at different abutments. An experimental study in dogs. *J. Clin. Periodontol.* **1998**, *25*, 721–727. [CrossRef]
16. Nevins, M.; Camelo, M.; Nevins, M.L.; Schupbach, P.; Kim, D.M. Connective tissue attachment to laser-microgrooved abut-ments: A human histologic case report. *Int. J. Periodontics Restor. Dent.* **2012**, *32*, 385–392.
17. Romanos, G.E.; Traini, T.; Johansson, C.B.; Piattelli, A. Biologic Width and Morphologic Characteristics of Soft Tissues Around Immediately Loaded Implants: Studies Performed on Human Autopsy Specimens. *J. Periodontol.* **2010**, *81*, 70–78. [CrossRef]
18. Giuliani, A.; Cedola, A. Advanced high-resolution tomography in regenerative Medicine. In *Three-Dimensional Exploration into the Interactions between Tissues, Cells, and Biomaterials*, 1st ed.; Springer: Cham, Switzerland, 2018.
19. Albertini, G.; Giuliani, A.; Komlev, V.; Moroncini, F.; Pugnaloni, A.; Pennesi, G.; Belicchi, M.; Rubini, C.; Rustichelli, F.; Tasso, R.; et al. Organization of Extracellular Matrix Fibers Within Polyglycolic Acid–Polylactic Acid Scaffolds Analyzed Using X-Ray Synchrotron-Radiation Phase-Contrast Micro Computed Tomography. *Tissue Eng. Part C Methods* **2009**, *15*, 403–411. [CrossRef]
20. Giuliani, A.; Moroncini, F.; Mazzoni, S.; Belicchi, M.L.; Villa, C.; Erratico, S.; Colombo, E.; Calcaterra, F.; Brambilla, L.; Torrente, Y.; et al. Polyglycolic Acid-Polylactic Acid Scaffold Response to Different Progenitor Cell In Vitro Cultures: A Demonstrative and Comparative X-Ray Synchrotron Radiation Phase-Contrast Microtomography Study. *Tissue Eng. Part C Methods* **2014**, *20*, 308–316. [CrossRef]
21. Giuliani, A.; Greco, S.; Pacilè, S.; Zannotti, A.; Carpini, G.D.; Tromba, G.; Giannubilo, S.R.; Ciavattini, A.; Ciarmela, P. Advanced 3D Imaging of Uterine Leiomyoma's Morphology by Propagation-based Phase-Contrast Microtomography. *Sci. Rep.* **2019**, *9*, 10580. [CrossRef]
22. Bravin, A.; Coan, P.; Suortti, P. X-ray phase-contrast imaging: From pre-clinical applications towards clinics. *Phys. Med. Biol.* **2012**, *58*, R1–R35. [CrossRef]
23. Brun, F.; Massimi, L.; Fratini, M.; Dreossi, D.; Billé, F.; Accardo, A.; Pugliese, R.; Cedola, A. SYRMEP Tomo Project: A graphical user interface for customizing CT reconstruction workflows. *Adv. Struct. Chem. Imaging* **2017**, *3*, 1–9. [CrossRef]
24. Paganin, D.; Mayo, S.C.; Gureyev, T.E.; Miller, P.R.; Wilkins, S.W. Simultaneous phase and amplitude extraction from a single defocused image of a homogeneous object. *J. Microsc.* **2002**, *206*, 33–40. [CrossRef]
25. Drezner, M.K.; Glorieux, F.H.; Kanis, J.A.; Malluche, H.; Meunier, P.J.; Ott, S.M.; Recker, R.R. Bone histomorphometry: Standard-ization of nomenclature, symbols, and units: Report of the asbmr histomorphometry nomenclature committee. *J. Bone Min. Res.* **1987**, *2*, 595–610. [CrossRef]
26. Fazzalari, N.L.; Parkinson, I.H. Fractal dimension and architecture of trabecular bone. *J. Pathol.* **1996**, *178*, 100–105. [CrossRef]

27. Bolle, C.; Felice, P.; Barausse, C.; Pistilli, V.; Trullenque-Eriksson, A.; Esposito, M. Four mm long vs longer implants in aug-mented bone in posterior atrophic jaws: 1-year post-loading results from a multicentre randomised controlled trial. *Eur. J. Oral Implant.* **2018**, *11*, 31–47.
28. Brauer, E.; Lippens, E.; Klein, O.; Nebrich, G.; Schreivogel, S.; Korus, G.; Duda, G.N.; Petersen, A. Collagen Fibrils Mechanically Contribute to Tissue Contraction in an In Vitro Wound Healing Scenario. *Adv. Sci.* **2019**, *6*, 1801780. [CrossRef] [PubMed]
29. Alberich-Bayarri, A.; Marti-Bonmati, L.; Angeles Pérez, M.; Sanz-Requena, R.; Lerma-Garrido, J.J.; García-Martí, G.; Moratal, D. Assessment of 2D and 3D fractal dimension measurements of trabecular bone from high-spatial resolution magnetic reso-nance images at 3 T. *Med. Phys.* **2010**, *37*, 4930–4937. [CrossRef] [PubMed]
30. Meyer, M. Processing of collagen based biomaterials and the resulting materials properties. *Biomed. Eng. Online* **2019**, *18*, 1–74. [CrossRef] [PubMed]
31. Parry, D.A. The molecular fibrillar structure of collagen and its relationship to the mechanical properties of connective tissue. *Biophys. Chem.* **1988**, *29*, 195–209. [CrossRef]
32. Kayed, H.R.; Kirby, N.; Hawley, A.; Mudie, S.T.; Haverkamp, R.G. Collagen fibril strain, recruitment and orientation for pericardium under tension and the effect of cross links. *RSC Adv.* **2015**, *5*, 103703–103712. [CrossRef]
33. Hinz, B. The myofibroblast: Paradigm for a mechanically active cell. *J. Biomech.* **2010**, *43*, 146–155. [CrossRef]
34. Mangano, C.; Piattelli, A.; Mangano, F.; Rustichelli, F.; Shibli, J.A.; Iezzi, G.; Giuliani, A. Histological and Synchrotron Radia-tion-Based Computed Microtomography Study of 2 Human-Retrieved Direct Laser Metal Formed Titanium Implants. *Implant Dent.* **2013**, *22*, 175–181. [CrossRef]
35. Manescu, A.; Giuliani, A.; Mohammadi, S.; Tromba, G.; Mazzoni, S.; Diomede, F.; Zini, N.; Piattelli, A.; Trubiani, O. Osteogenic potential of dualblocks cultured with human periodontal ligament stem cells: In vitro and synchrotron microtomography study. *J. Periodontal Res.* **2016**, *51*, 112–124. [CrossRef]
36. Mazzoni, S.; Mohammadi, S.; Tromba, G.; Diomede, F.; Piattelli, A.; Trubiani, O.; Giuliani, A. Role of cortico-cancellous heterologous bone in human periodontal ligament stem cell xeno-free culture studied by Synchrotron radiation phase-contrast microtomography. *Int. J. Mol. Sci.* **2017**, *18*, 364. [CrossRef]